Supporting information for

Novel sintering and band gap engineering of ZnTiO$_3$ ceramics with excellent microwave dielectric properties

Shenhui Lei†, Huiqing Fan*†, Xiaohu Ren†, Jiawen Fang‡, Longtao, Ma†, Zhiyong Liu†

† State Key Laboratory of Solidification Processing, School of Materials Science and Engineering, Northwestern Polytechnical University, Xi'an 710072, China

‡ Institute for Superconducting and Electronic Materials, University of Wollongong, NSW 2522, Australia

Corresponding Author

* E-mail: *leishenhui@163.com* **and** *hqfan3@163.com.* **Tel.:** *+86 29 88494463*; **fax:** *+86 29 88492642.*

As is well acknowledged, ZnTiO$_3$ ceramic is very sensitive to temperature and experimental conditions. The SEM images of ceramics presintered at variable temperatures 750-850 °C are shown in Fig. S1. It is found that the low temperature phase Zn$_2$Ti$_3$O$_8$ is largely reduced with a long holding time (4-5 h) at a proper low presintering temperature (800 °C). From Fig. S1(b), it is apparent that the reaction of phase transition happened at 900 °C can be divided into 2 parts, and the former reaction happened fast with a steep slope shown in the DSC curve, which can be attributed to the constituent fluctuation caused by migration of Ti ions. The latter reaction takes a long time for the conversion to complete, which is related to the difficult and accumulating process of nucleation and growth of the second phase.

Generally, the Zn$_2$Ti$_3$O$_8$ phase is thought to be an intermediate phase. With the component modulating of Ti element, Zn$_2$Ti$_3$O$_8$ phase is largely suppressed at 850 °C/3 h. Thus, the Zn$_2$Ti$_3$O$_8$ phase is proved to be a Ti-defect dominant phase, and as far as we concern, this is reported for the first time. The ratio of Ti to Zn (x) is important to reduce the low temperature phase Zn$_2$Ti$_3$O$_8$. As can be seen in Fig S2, the content of Zn$_2$Ti$_3$O$_8$ is as high as 24.052% at x=0.9. While at x=1.1, the content of Zn$_2$Ti$_3$O$_8$ decreases to 1.618%. The percentage of content is calculated by the following equation:

$$Content_{ZnTiO_3} = \frac{I_{ZnTiO_3(311)} + I_{ZnTiO_3(440)}}{I_{ZnTiO_3(311)} + I_{ZnTiO_3(440)} + I_{Zn_2Ti_3O_8(311)} + I_{Zn_2Ti_3O_8(220)} + I_{TiO_2(110)} + I_{TiO_2(211)}}$$

$$ \text{(1)} $$

$$ Content_{Zn_2Ti_3O_8} = 1 - Content_{ZnTiO_3} - Content_{TiO_2} \qquad \text{(2)} $$

Where the $I_{ZnTiO3\ (311)}$, $I_{ZnTiO3\ (440)}$, $I_{Zn2Ti3O8\ (311)}$ and $I_{Zn2Ti3O8\ (220)}$ are characteristic peak area corresponding to the two XRD diffraction peaks index to $ZnTiO_3$ and $Zn_2Ti_3O_8$ phase with the highest intensity, respectively.

Excellent microwave dielectric properties are obtianed in the novel $ZnTiO_3$ ceramic after introduction of ZnO nano additives. We investigate the results further to reveal the deep mechnism of this largely imporved propeties and confirm these results. The homogeneous ZnO nano particles with uniform size of 10-15 nm are successfully prepared via simple solution synthesis by using $Zn(NO_3)_2 \cdot 6H_2O$, NaOH and CDTA(Cyclohexane-diamine-tetraacetic Acid). The mixed solution is heated at 140 °C for 0.5-4 h, after centrifugation and vacuum drying, the properties of ZnO nano particles are tested. The schematic diagram of experimental facilities for preparing ZnO nanostructures by low temperature solution method is shown in Fig. S3. The morphology of the prepared nano ZnO is examined by TEM. (Fig. S4). It reveals the relationship between the particles size of ZnO nanostructures and the amount of CDTA. Fig. S4(a) is the corresponding bright-field TEM images of the products. It can be seen from the TEM images that the products are all regular disc-like with a narrow distribution of size, 13-15 nm, and the nano ZnO particles are composed of single-crystalline structure. Fig. S4(c) is the corresponding high resolution TEM (HRTEM) image, and it shows that the nanoparticles are well crystallized and isotropous. Fig. S4(d), the SAED patterns, is composed of polycrystalline diffraction rings, indicating the nanocrystalline nature of particles. The concentric diffraction rings from inside to outside correspond well to the (100), (002), (101), (102) and (110) reflections of hexagonal ZnO (JCPDS No. 36-1451).

Based upon aforementioned analysis, band alignments, including the valence band and conduction band, have also been conducted and presented in Fig. S7(e). The UV-vis absorption spectra demonstrates clearly the intrinsic light absorption edge, and the larger bandgap of 0.14 eV of ZnO compared to $ZnTiO_3$ is further confirmed by the fluorescence emission spectrum as a 15 nm shift in Fig. S5. Furthermore,

photoluminescence (PL) emission spectra is also obtained to confirm the results above. As exhibited in Fig. S5, the strong photoluminescence emission peaks for $ZnTiO_3$, ZnO assigned to radiative recombination of charge carriers can be observed. The position of the peaks are consistent with the UV-vis diffuse reflection spectra. Particularly, the addition of nano ZnO can cause a suppressed electron transfer process.

The $ZnTiO_3$ ceramic achieved in this work is different from the previously reported ones regarding the pure structures obtained above the phase transition temperature (without secondary phase Zn_2TiO_4 and TiO_2). The improved features are undoubtedly related to the homogenous structures; thus, the Rietveld refinement is carried out with the R$\underline{3}$ (No.148) space group at room temperature, by using the GSAS-EXPGUI program[7,8]. The XRD data is collected in the 2θ range of 10-130° with a step of 0.02° and a step time of 10 s. The coordinates of hexagonal $MgTiO_3$ with space group R$\underline{3}$ and cubic Zn_2TiO_4 with space group Fd$\underline{3}$m are used as initial model, respectively. The results are exhibited in the Fig. S6. For $ZnTiO_3$, Zn (5%) and Ti (5%) occupied the Ti (6c) and Zn (6c) site, respectively. The 6c site is the 6-fold Wyckoff positions. So this has a negligible effects on the microstructures. The final refined profiles for pure $ZnTiO_3$ are shown in Fig. S6. The crystallographic data, R factors and experimental conditions are listed in Table. S1. The final factors, R_p, R_{wp} and chi-squared values (χ^2) are 6.18%, 7.26%, and 1.352 for $ZnTiO_3$. The refined lattice parameters are a=5.1456 Å, b=5.1456 Å, c=14.0234 Å. Table. S3 lists the atomic coordinates, atomic occupancies and isotropic thermal parameters of $ZnTiO_3$, respectively.

The same Rietveld refinement is also carried out for the Zn_2TiO_4 phase. And the results confirm the Zn_2TiO_4 phase has a cubic inverse spinel structure with the space group Fd$\underline{3}$m. The crystallographic data, R factors and experimental conditions are also listed in Table. S1. The final factors, R_p, R_{wp} and chi-squared values (χ^2) are 5.56 %, 6.89 %, and 1.611 for Zn_2TiO_4. The refined lattice parameters are a=8.4856 Å. Table. S2 and Table. S3 exhibit the atomic coordinates, atomic occupancies and isotropic thermal parameters of $ZnTiO_3$ and Zn_2TiO_4, respectively.

The schematic diagrams of the structures to $ZnTiO_3$ phase and Zn_2TiO_4 phase are illustrated in Fig. S9. The $ZnTiO_3$ phase has a hexagonal perovskite structure, while the

Zn_2TiO_4 phase has inverse spinel structure rather than the spinel structure, as the A and B blocks have apparent differences. In the inverse spinel structure Zn^{2+} ions are occupied the tetrahedral interstice position and half of the octahedral interstice position. These results certify that the secondary phase Zn_2TiO_4 and its parent phase $ZnTiO_3$ have different structure. It also proved that edge-connected TiO_6 octahedra exists in the $ZnTiO_3$ phase and corner-connected TiO_6 octahedra in Zn_2TiO_4 phase, in accordance with the Raman spectrums in Fig. 4.

Overall, the analysis aforementioned can prove that the new way of this method is an effective way to prepare the pure $ZnTiO_3$ material with a high performance, and the new devices based on this material will also exhibit promising operating characteristics for many applications. Thus, this pure $ZnTiO_3$ material could have broad chemical related applications such as gas sensors (ethanol, NO, CO etc.), green chemistry catalyst or photo catalyst, UV-screening agent, paint pigment and photoluminescence). Most importantly, it's believed that this new method could pave a new way for preparation of many materials that are difficult to be synthesize in a pure phase by creating a nano buffer regions, that is, stabilize the needed phase (especially for materials existing different phases, or sensitive to the composition, experimental conditions and temperature), such as $BiFeO_3$, $LiNiO_2$, $LiCoO_2$, Li_2MnO_3 or $LiMn_2O_4$, SnS_2, CdS, $CH_3NH_3PbI(Br,Cl)_3$, $CH_3NH_3(Pb,Sn)(I,Br)_3$, in the hot frontiers: photovoltaic devices in ferroelectric, micro-electron-mechanical systems (MEMS) or very precise actuators, anode/cathode materials for Lithium-ion batteries, perovskite solar cells, new photo catalysts, hydrogen production from water, etc. The band structures and band engineering for the movement of carriers (electron and hole) can also pave a new way for synthesis of materials with devisable high performance by optimization of band structure (here, extraordinary low loss by introducing dispersive nano buffer regions with a wider band gap and a higher conduction band minimum; otherwise, large enhancement in the hole/electron transport or transfer process); thus, that can enable new desirable properties, e.g., high-capacity and long cycle time for a rechargeable Li-ion or Na-ion battery cell, highly efficient hydrogen evolution from water splitting, etc.

References

1 S. Yang, Y. Gong, J. Zhang, L. Zhan, L. Ma, Z. Fang, R. Vajtai, X. Wang, P.M. Ajayan, *Adv. Mater.* 2013, **25**, 2452-2456.

2 S.L. Rühle, K.V. Vugt, H.Y. Li, N.A. Keizer, L. Kuipers, D. Vanmaekelbergh, *Nano Lett.* 2008, **8**, 119‑123

3 J. Xu, X. Yang, H.K. Wang, X. Chen, C.Y. Luan, Z.X. Xu, Z.Z. Lu, V.A.L. Roy, W.J. Zhang, C.S. Lee, *Nano Lett.* 2011, **11**, 4138‑4143

4 C.R. Satish, K. Wang, Y. Ding, J. K. Marmon, M. Bhatt, Y. Zhang, W.L. Zhou, Z.L. Wang, *ACS Nano* 2015, **9**, 6419‑6427.

5 N. Pal, M. Paul, A. Bhaumik, *Appl. Catal. A* 2011, **393**, 153-160.

6 W.D. Leim, P.R. Dimova, M. Antonietti, *J. Am. Chem. Soc.* 2011, **133**, 7121-7127.

7 A.C. Larson, R.B. Von Dreele, General Structure Analysis System (GSAS), LANL Report LAUR 86-748, Los Alamos National Laboratoty, Los AlAmos, NM, 2000.

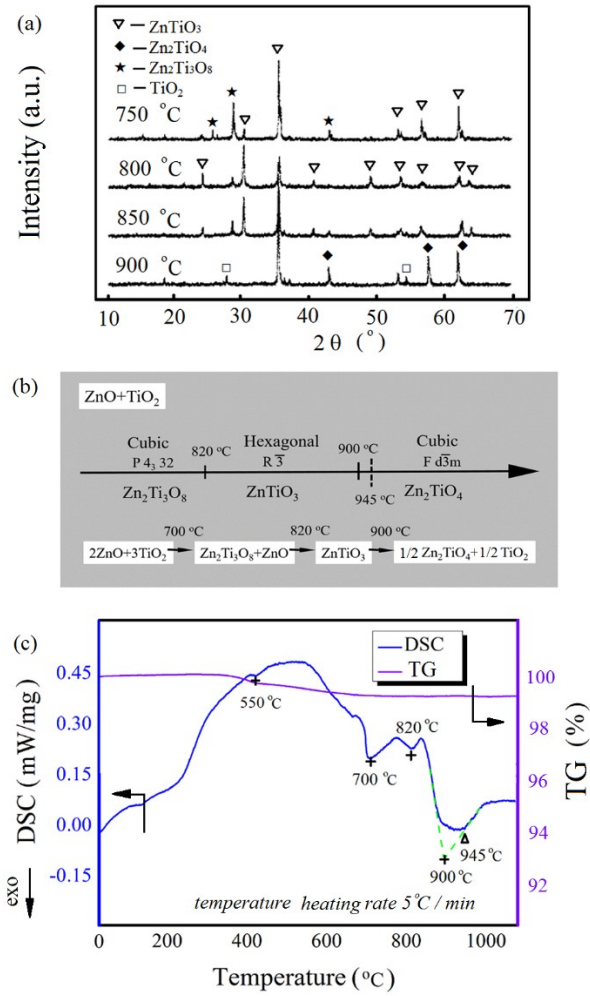8 B.H. ToBy, EXPGUI, a graphical user interface for GSAS. *J. Appl. Crystallogr.* 2001, **34**, 210-213.

Fig. S1 The schematic of the phase transition in ZnO-TiO$_2$ system with temperature dependent characteristic, (a) the XRD patterns of ZnO-TiO$_2$ (1:1) content at different sintering temperature for 3h, (b) the diagram of the phase transition with increasing temperature, (c) the DSC and TG curves at a scanning speed of 5 ℃/min.
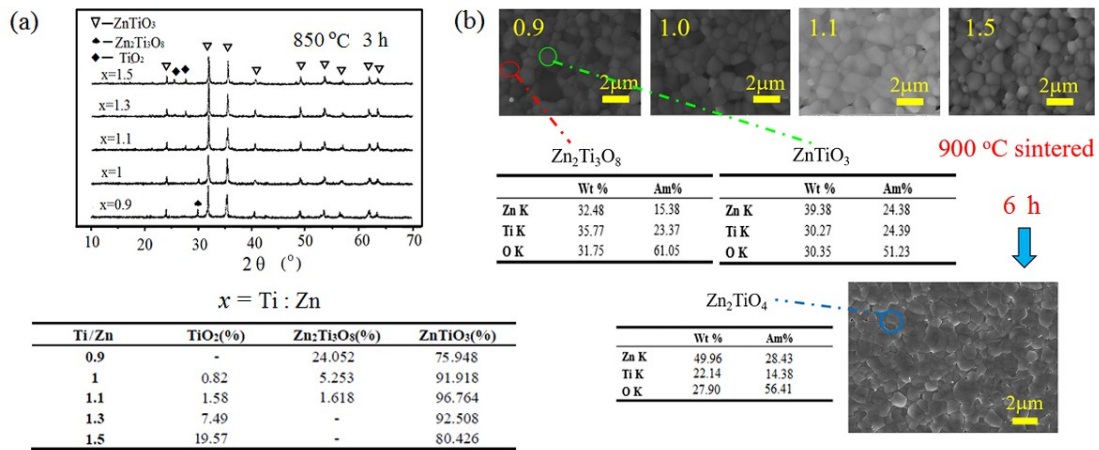
6

Fig. S2 (a) the composition to ZnO-TiO$_2$ ceramics with different x=Ti:Zn ratio (0.9, 1.0, 1.1, 1.3, 1.5), (b) the corresponding microstructure morphology and the EDS result of content to different x ratio (0.9, 1.0, 1.1, 1.5), respectively. With a long sintering time at 900 ^{o}C/6 h (below the phase transition temperature), the ZnTiO$_3$ phase has already transformed into Zn$_2$TiO$_4$ phase thoroughly.
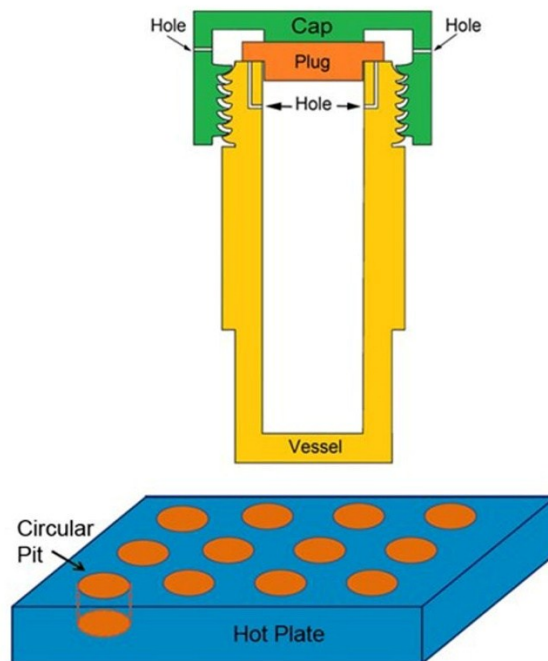

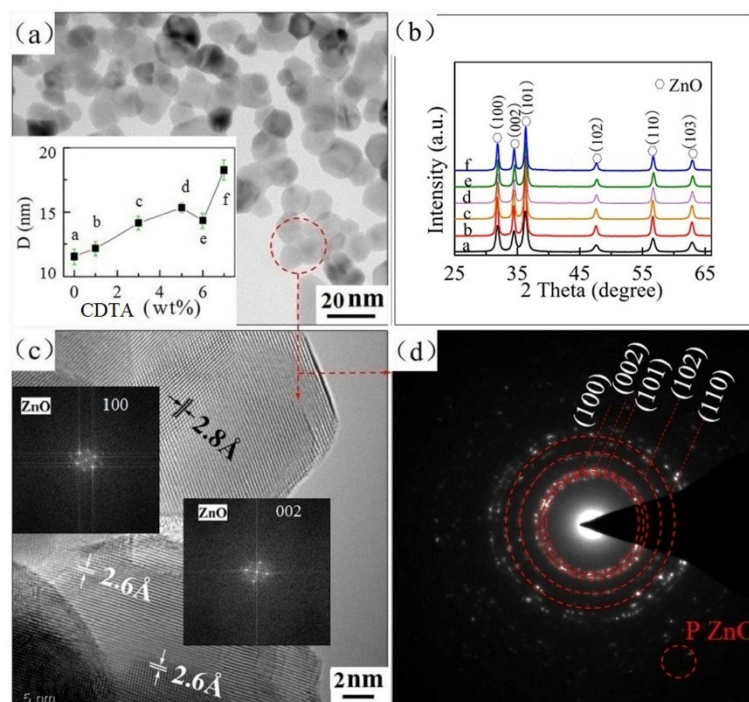Fig. S3 The schematic diagram of experimental facilities for preparing ZnO nanostructures by low temperature solution method

Fig. S4 (a) TEM images, the inset is the average crystal size (D) of the samples; (b) Powder XRD patterns with different CDTA concentrations (a-e refer to 0, 1, 3, 5, 6, 7 mol % CDTA, respectively); (c, d) HRTEM image and ED pattern corresponding to the marked frame area of ZnO nanostructure with 5 wt % CDTA (the insets is the FFT images of ZnO).
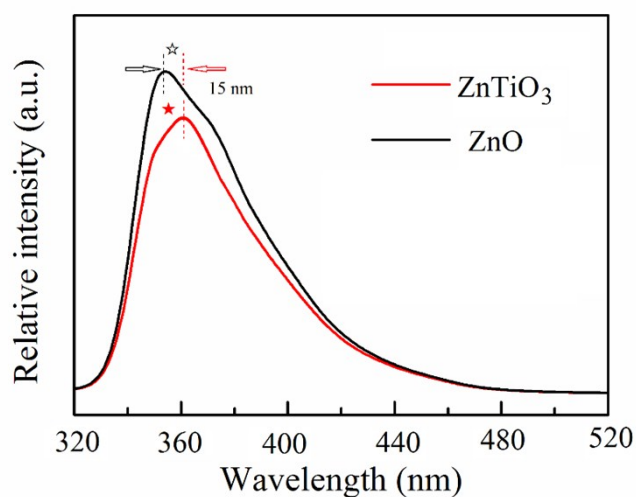

Fig. S5 Room temperature photoluminescence spectra of $ZnTiO_3$ and ZnO under 325 nm excitation.
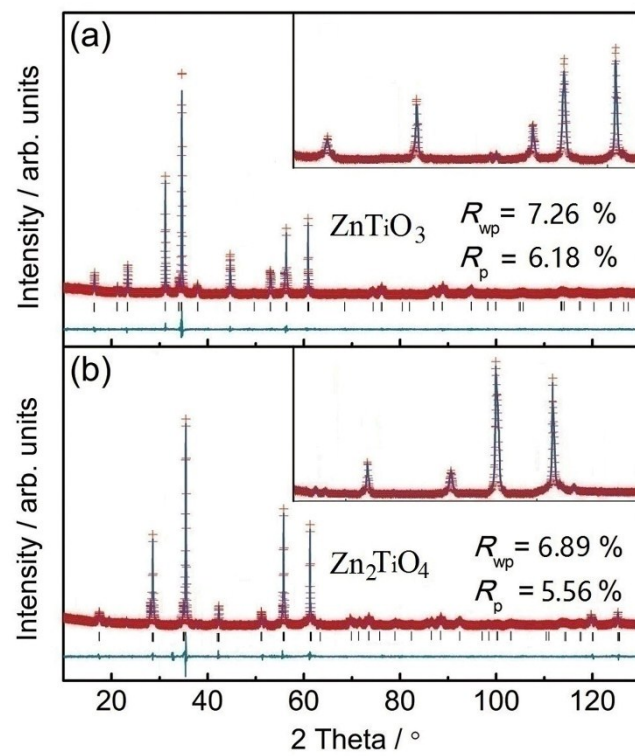
Fig. S6 Rietveld refinements for (a) $ZnTiO_3$ and (b) Zn_2TiO_4 at room temperature, with insets showing the regionally enlarged drawings.
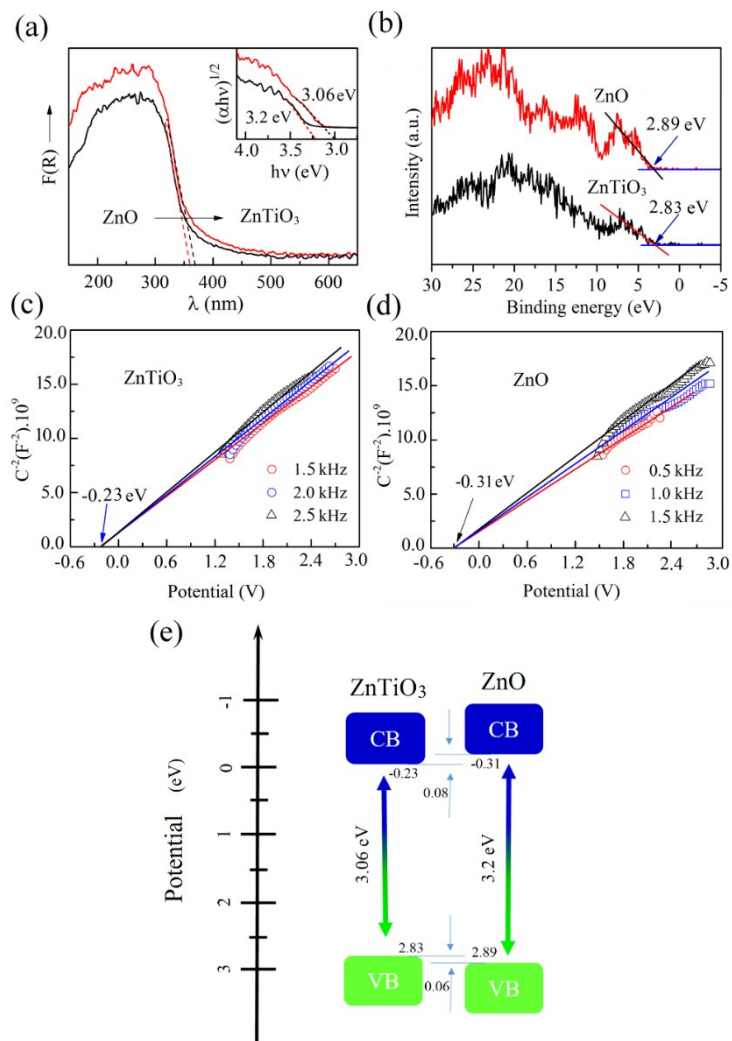
Fig.S7 (a) UV-vis diffuse reflectance spectra and (b) high-resolution valance band XPS spectra of ZnTiO$_3$ and ZnO; (c) electrochemical Mott-Schottky plots of ZnTiO$_3$; and (d) ZnO at selected frequencies; (e) electronic band structure of ZnTiO$_3$ and ZnO. Inset of (a): band gap determination from $(\alpha h \upsilon)^{1/2}$ versus photon-energy plot.
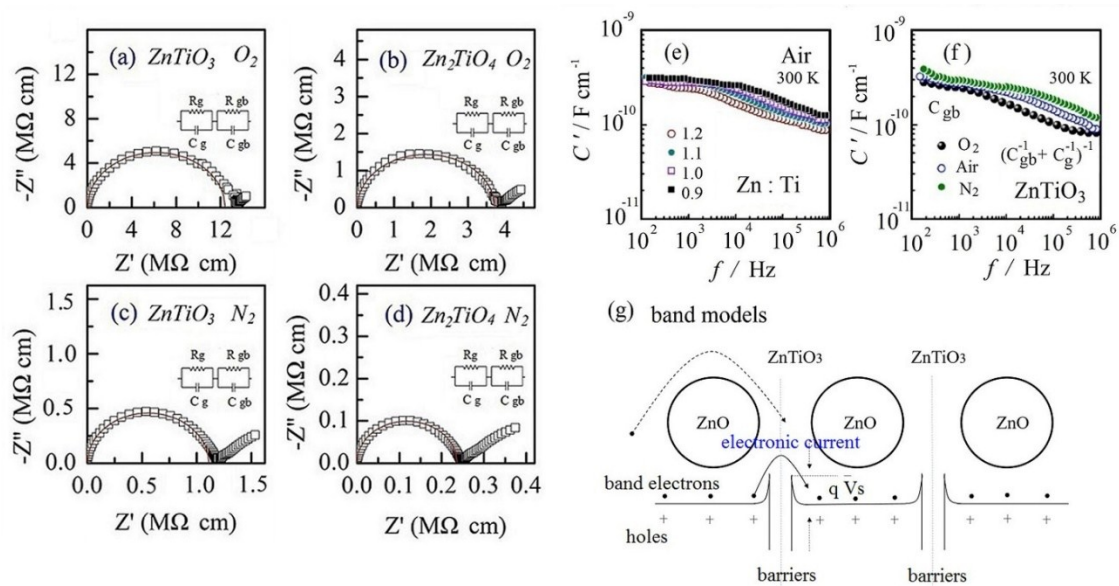
Fig. S8 (a-d) The Nyquist plots of the ZnTiO$_3$ ceramics with nano ZnO and Zn$_2$TiO$_4$ ceramic in O$_2$ and N$_2$ atmosphere, respectively. (e-f) capacitance C′ spectroscopic plot at room temperature for ZnTiO$_3$ ceramics with different Zn:Ti ratio annealed in air; comparison of capacitance C′ spectroscopic plot annealed in O$_2$, Air and N$_2$ for ceramic grain and grain boundary, respectively. (g) Band models for ZnTiO$_3$ ceramic with nano ZnO regions.
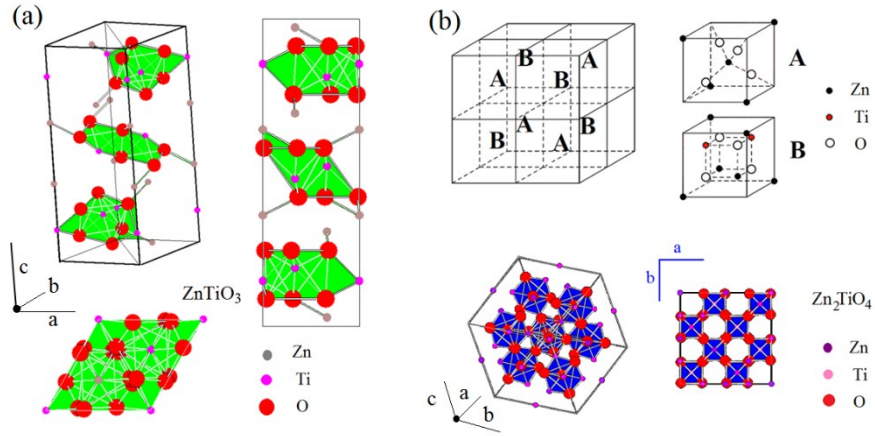
Fig. S9 the crystal structures to pure ZnTiO$_3$ phase and Zn$_2$TiO$_4$ phase, respectively. (a) ZnTiO$_3$ phase has a hexagonal structure in space group R$\underline{3}$, (b) Zn$_2$TiO$_4$ phase has a cubic inverse spinel structure in Fd$\underline{3}$m space group. The A and B blocks as shown make up the basic units for a unit cell.

Table. S1 Crystal data and structure refinement conditions for ZnTiO$_3$ and Zn$_2$TiO$_4$

Compound reference	ZnTiO$_3$	Zn$_2$TiO$_4$
Chemical formula	ZnTiO$_3$	Zn$_2$TiO$_4$
Formula mass	161.2742	242.6826
Crystal system	Hexagonal	Cubic
a (Å)	5.1456	8.4856
b (Å)	5.1456	8.4856
c (Å)	14.0234	8.4856
V (Å^3)	371.3003(5)	611.0090(8)
T (k)	298	298
Space group	R$\underline{3}$(No 148)	Fd$\underline{3}$m
No. of formula units per unit cell, Z	6	8
No. of data points	6000	6000
Reduced χ^2	1.352	1.611
R_{int} (%)	3.2	3.8
R_{wp} (%)	7.26	6.89
R_p (%)	6.18	5.56

Table. S2 Atomic coordinates, atomic occupancies and isotropic thermal parameters for ZnTiO$_3$ at room temperature

Atom	Site	x	y	z	100 U_{iso} (Å^2)	Occupancy
Zn1	6c	0	0	0.36175	0.0050	1
Ti1	6c	0	0	0.14840	0.0068	1
O1	18f	0.32125	0.02324	0.24755	0.0090	1

Table. S3 Atomic coordinates, atomic occupancies and isotropic thermal parameters for Zn$_2$TiO$_4$ at room temperature

Atom	Site	x	y	z	100 U_{iso} (Å^2)	Occupancy
Zn1	8a	1/8	1/8	1/8	0.0026	0.998
Ti1	8a	1/8	1/8	1/8	0.0026	0.002
Zn2	16d	1/2	1/2	1/2	0.0038	0.495
Ti2	16d	1/2	1/2	1/2	0.0038	0.505
O1	32e	0.26060	0.26060	0.26060	0.0115	1